Title

Coronene-Based Graphene Nanoribbons Insulated by Boron Nitride Nanotubes: Electronic Properties of the Hybrid Structure.

Journal

ACS omega, 3(10)

ISSN

2470-1343

Authors

Gracia-Espino, Eduardo
Barzegar, Hamid Reza
Zettl, Alex

Publication Date

2018-10-01

DOI

10.1021/acsomega.8b01617

Peer reviewed

ACS OMEGA

Article

Cite This: ACS Omega 2018, 3, 12930−12935

http://pubs.acs.org/journal/acsodf

Coronene-Based Graphene Nanoribbons Insulated by Boron Nitride Nanotubes: Electronic Properties of the Hybrid Structure

Eduardo Gracia-Espino,[†] Hamid Reza Barzegar,*[,†,‡] and Alex Zettl*[,‡,§,∥]

[†]Department of Physics, Umea University, 90187 Umea, Sweden

[‡]Department of Physics, University of California, Berkeley, California 94720, United States

[§]Materials Sciences Division, Lawrence Berkeley National Laboratory, Berkeley, California 94720, United States

[∥]Kavli Energy Nano Sciences Institute, The University of California, Berkeley and the Lawrence Berkeley National Laboratory, Berkeley, California 94720, United States

Supporting Information

ABSTRACT: We present a theoretical study on the formation of graphene nanoribbons—via polymerization of coronene molecules—inside the inner cavity of boron nitride nanotubes. We examine the electronic property of the hybrid system, and we show that the boron nitride nanotube does not significantly alter the electronic properties of the encapsulated graphene nanoribbon. Motivated by previous experimental works, we examine graphene nanoribbons with two different widths and investigate probable scenarios for defect formation and/or twisting of the resulting graphene nanoribbons and their effect on the electronic properties of the hybrid system.

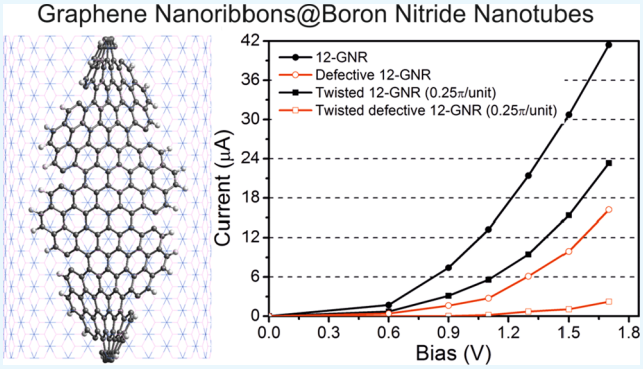

INTRODUCTION

Graphene nanoribbons (GNRs) with a tunable band gap, as a function of width and edge configurations, are promising candidates for future nanoscale electronic devices.[1−8] GNRs can be obtained via a top-down procedure by selectively cutting graphene sheets[9,10] or unzipping carbon nanotubes,[11−13] or in a bottom-up fashion via polymerization of small carbon-based molecules (molecular building blocks).[14−18] The latter is a more promising approach because it offers better control over the width and edge configuration of GNRs and the possibility for band gap engineering.[19,20] The polymerization of the molecular building blocks is usually catalyzed by an underlying thin film of Au or Ag,[17,19] or promoted by constraining the building blocks to a regular arrangement in the inner cavity of nanotubes.[15,16,21−23] Although the former approach (utilizing catalysts) provides defect-free GNRs with well-defined edges, there is no control over quantity, orientation, and length of the synthesized GNRs; additionally, because of strong adhesion between the GNR and the underlying metallic thin film, it is challenging to transfer the GNRs to another substrate of choice. In contrast, the latter approach provides individual GNRs inside nanotubes, where the GNR width, and to some extent also length, are determined, respectively, by the diameter and the length of the host nanotube.

It is known that the interaction of nanostructures with the surrounding environment, in particular a substrate, can alter associated electronic properties.[24,25] Therefore, freestanding (isolated) nanostructures under an inert atmosphere might appear to be a preferred configuration for nanodevice fabrication. However, such a geometry is extremely challenging for practical technological applications. The encapsulation of GNRs in the inner cavity of single-walled carbon nanotubes (SWCNT) overcomes some of the difficulties, but because SWCNTs are electronically active materials, they may negatively alter the properties of the GNR and its function in electronic devices. We recently reported the synthesis of GNRs in the inner cavity of boron nitride nanotubes (BNNTs),[26] via polymerization of coronene molecules, in which the high chemical and thermal resistance of BNNTs protects the encapsulated GNR from ambient degradation. The host BNNT, with a large electronic band gap, presumably also acts as an electrically insulation layer for the encapsulated GNRs, which in turn suggests a route for practical implementation in integrated circuits.

Here, we theoretically probe such hypotheses by means of density functional theory (DFT). We study the encapsulation and structure of coronene-based GNRs inside the inner cavity of BNNTs and show that encapsulated GNRs do not significantly interact electronically with the surrounding BNNT. We also examine different intermolecular interactions between coronenes and possible defect formation and

Received: August 16, 2018
Accepted: September 24, 2018
Published: October 10, 2018

DOI: 10.1021/acsomega.8b01617
ACS Omega 2018, 3, 12930−12935

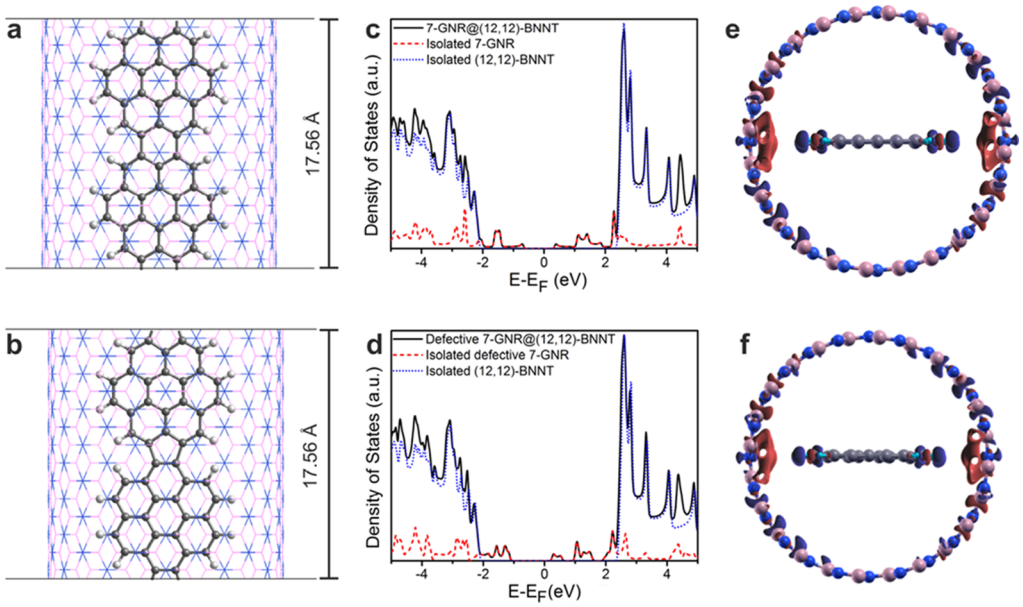

Figure 1. (a) Pristine and (b) defective 7-GNRs@(12,12)-BNNT hybrid structure. DOS of the isolated GNR, isolated BNNT, and the 7-GNR@(12,12)-BNNT hybrid structure for (c) pristine case and (d) defective case. Charge redistribution after introducing the (e) pristine 7-GNRs and (f) defective 7-GNR into the (12,12)-BNNT. Red (blue) indicates electron accumulation (depletion). The iso-surfaces are plotted at 0.00005 eV/Å^3 to see the effect; however, the charge transfer is negligible.

consequent effects on the electronic properties of the host GNRs.

RESULTS AND DISCUSSION

Encapsulated GNRs inside BNNTs. Coronene is a symmetric flat carbon-based molecule, in which the carbon atoms at the edges form periodic zigzag−armchair configurations. The polymerization of coronene molecules (confined within the inner cavity of a BNNT) forms a nonmagnetic semiconductor GNR with irregular edges (see Figure 1a,b). The chemical bonding between two coronene molecules can be realized either by formation of a hexagonal ring (when two zigzag edges are facing each other, see Figure 1a) or via a pentagonal ring (when a zigzag edge faces an armchair edge, see Figure 1b). The former results in the growth of a defect-free GNR with an electronic band gap (E_g) of 0.92 eV and a lattice parameter (along the growth direction) of 8.65 Å. The latter case, on the other hand, results in the formation of a defective GNR with a larger E_g of 1.52 eV (see Figure 1c,d). In both cases, the resulting GNR is seven carbon atoms wide at its wider part; therefore, we denote this GNR as "7-GNR" in the text. In both cases, the resulting GNRs have irregular edges, with a mixture of zigzag and armchair sides and a nonuniform width along the length of the GNR.[4]

The interaction between encapsulated GNRs and BNNTs is theoretically investigated by introducing GNRs into a (12,12)-BNNT (7-GNR@(12,12)-BNNTs). The (12,12)-BNNT exhibits an E_g equal to 4.70 eV, which is in agreement with previous reports,[27,28] and has a diameter of 16.5 Å, which ensures a minimum separation distance of 3.6 Å from the GNR. There is a natural mismatch between the lattice parameter along the growth direction of BNNTs and the coronene-based GNRs. Thus, a supercell comprising a coronene dimer (dicoronylene) and seven BNNT unit cells is used, resulting in a lattice mismatch of 0.29 Å. This change in the lattice parameter slightly increases the band gap, but its effect on the electronic properties is insignificant as seen in Figure S1. The optimized geometries of both composite systems, pristine and defective 7-GNRs@(12,12)-BNNTs, are depicted in Figure 1a,b. The interaction between GNRs and the BNNT seems negligible, as the density of states (DOS) of the composite system is basically a combination of both isolated components (see Figure 1c,d). The charge density transfer ($\delta n(r)$) is computed by performing a Bader charge analysis on the composite and the individual components, the results of which are shown in Figure 1e,f. As expected, the atoms located at the ribbon's edge interact most strongly with the BNNT's wall, but the charge transfer is 100 times smaller than that observed for metal−carbon interfaces,[29,30] and such a small charge transfer does not appreciably modify the electronic properties of the 7-GNRs@(12,12)-BNNTs.

GNRs may also form via polymerization of dicoronylene molecules (dimers of coronene) inside BNNTs of appropriate diameters.[26] As depicted in Figure 2a, the likely polymerization of dicoronylene molecules follows a regular pattern, in which the long, in-plane axis of the molecules makes an angle of 30° with respect to its zigzag vertical direction. The resulting GNR is 12 carbon atoms wide at its wider section, and therefore, we denote it as the "pristine 12-GNR" in the text. A defective 12-GNR can also be constructed by using the defective dicoronylene (in which the two coronenes are chemically bonded together via a pentagon; see the previous section). As illustrated in Figure 2b, the boundary between two defective dicoronylene molecules contains 7- and 5-member carbon rings. The pristine 12-GNR exhibits semiconductor behavior with a small E_g of 0.43 eV, whereas the defective 12-GNR exhibits a larger E_g of 0.75 eV and new localized states above and below the Fermi level because of introduced defects. For 12-GNRs, a (16,16)-BNNT is selected as a host with an E_g equal to 5.64 eV and a diameter of ∼22 Å, allowing a graphene-tube separation distance of 3.3 Å. The optimized structures are depicted in Figure S2. The DOS of both composite systems are plotted in Figure 2c,d. Similar to the 7-GNRs case, these results indicate that the interaction between

DOI: 10.1021/acsomega.8b01617
ACS Omega 2018, 3, 12930−12935

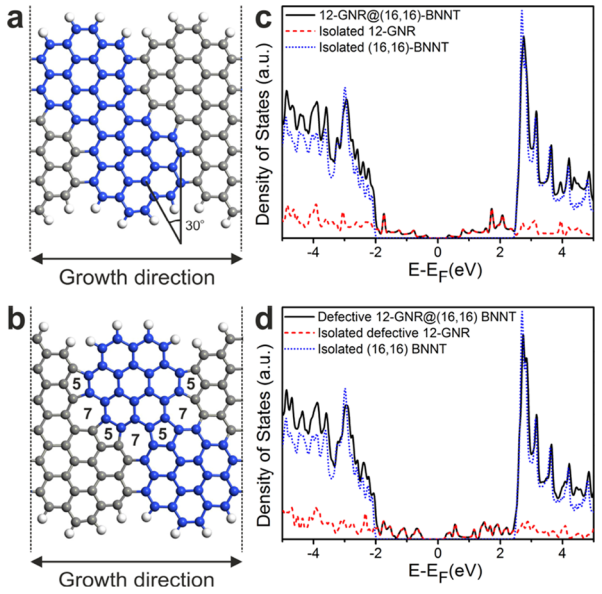

Figure 2. (a) Pristine and (b) defective 12-GNRs formed via polymerization of dicoronylene molecules. DOS of the isolated 12-GNR, isolated BNNT, and the 12-GNR@(16,16)-BNNT hybrid structure for (c) pristine case and (d) defective case. The carbon atoms in blue identify a dicoronylene molecule unit within the 12-GNR.

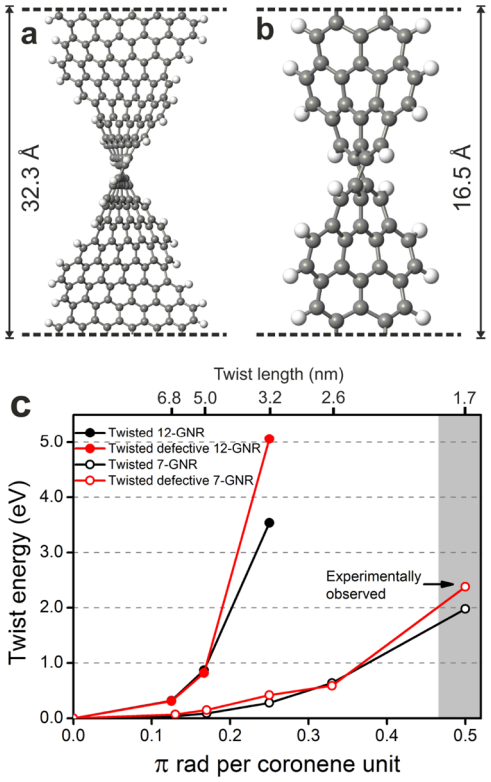

Figure 3. (a,b) Optimized structures of nondefective but twisted 12-GNR and 7-GNR at 0.25 and 0.5π rad/unit, respectively. (c) Energy required for a half-turn (180°) at different twisting rates.

the (16,16)-BNNT and the 12-GNR is negligible. Similar results are observed when encapsulating purely zigzag or armchair GNRs inside BNNTs, see Figure S3, clearly indicating that the edge morphology does not play a significantly role in the interaction with the nanotube.

Twisted GNRs. It has been shown that a freestanding GNR may experience twisting along its axis with a well-defined periodicity.[31,32] Such twisting is explained either by nonuniform stress along the length of the GNRs because of the elongation of the edges relative to the center of the GNR,[33,34] or by compressive strain.[35] Similarly, a GNR, encapsulated inside a nanotube, may also exhibit twisting along the host tube axis.[14,15,26,36] Below, we study such a possibility for GNRs encapsulated in BNNTs and investigate the properties of the resulting configurations.

The considered GNRs are twisted by 180° (1π rad) at different twisting rates (π rad/unit). Figure 3a,b depicts the optimized geometry of the nondefective 7- and 12-GNRs (see Figure S4 for more information). The energy necessary to achieve 1π rad (twist energy) is calculated as the energy difference between the flat and twisted configuration, and the results for different twisting rates are plotted in Figure 3c. In general, the twist energy is an increasing function of the twisting rate. For the narrow 7-GNRs, the increase in energy is relatively small when the twist occurs slowly (for instance, at a twist rate of 0.25π rad/unit, the GNR completes a full twist over a length of 3.25 nm, which requires an energy of 0.28 eV); however, it significantly increases for a higher twisting rate (e.g., 2 eV at 0.5π rad/unit). The electronic band gap of the twisted 7-GNRs exhibits a gradual increase from 0.92 eV at a twist rate equal to zero, up to 1.41 eV at a twist rate of 0.5π rad/unit; see Figure S5. For defective 7-GNRs, the increase in energy is similar at low twisting rates when compared to the nondefective case (it makes little or no difference), and only at a twist rate equal to 0.5π rad/unit, a significant difference in energy becomes apparent (increase by 0.36 eV). Regarding the band gap, the defective 7-GNR exhibits a reduction from 1.52 to 1.18 eV (Figure S6). However, this reduction is not beneficial for electron transport as discussed below. In fact, the reduced band gap is because of the appearance of localized electronic states that act as scattering states, degrading the electron transport, but enhancing the chemical reactivity. The experimentally observed twisted GNR exhibited a nonperiodic twisting with a twist length of approximately 1.7 nm,[26] which corresponds to a twist rate of 0.5π rad/unit. In Figure 3c, the region corresponding to experimental observation is indicated in gray, suggesting that such twisting is energetically less probable compared to other examined cases. The fact that the experimentally observed twisting for the encapsulated GNR is not periodic suggests that the origin of the twist is different from that for freestanding GNRs,[34,35] and is possibly induced by formation of a local defective side. Polymerization of coronene molecules can initiate from different points along the length of the nanotube, which in turn result in the formation of several GNR fragments (possibly with a slightly different orientation). This induces defected (twisted) regions when the small GNRs join together.

For the case of the wider 12-GNRs, the twist energy is significantly larger even at low twist rates (for instance, at 0.25π rad/unit, the twist energy is 3.54 eV), suggesting that such cases might not be physically realizable. This is rationalized by the internal strain accumulated by the atoms in the basal plane, while the 7-GNR can cope easily with such strain because of the single hexagonal (or pentagonal) carbon ring that joins the coronene units. The twisted 12-GNR exhibits a gradual increase in the band gap from 0.43 eV at twist rate zero up to 0.62 eV at a twist rate of 0.25π rad/unit; see Figure S7. The defective 12-GNR exhibits a slight increase

DOI: 10.1021/acsomega.8b01617
ACS Omega 2018, 3, 12930−12935

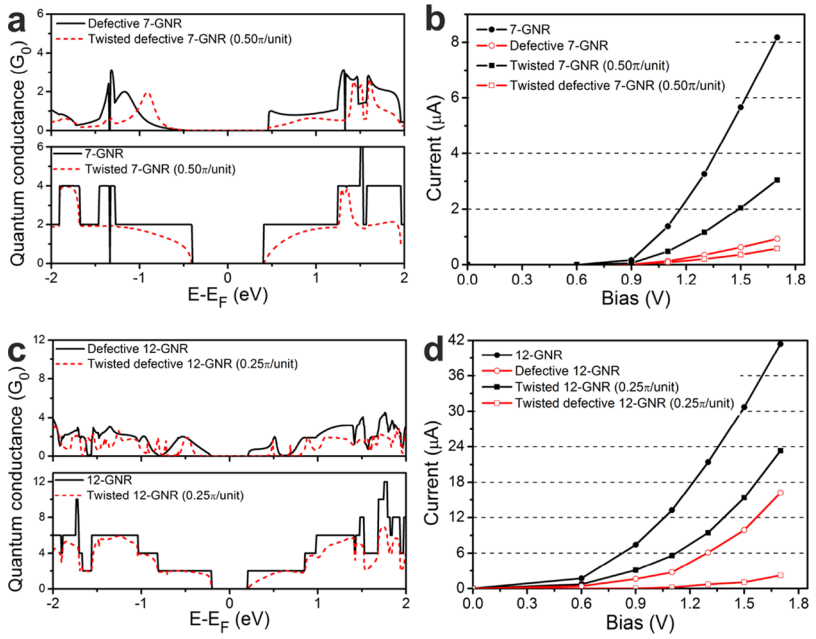

Figure 4. (a,c) TF ($G_0 = 2e^2/h$) and (b,d) $I-V$ characteristics of planar and twisted 7-GNRs and 12-GNRs.

in E_g; however, at the maximum twist rate of 0.25π rad/unit, two large peaks appear at the Fermi level (FL) associated to large internal strain located at the pentagonal carbon rings, where the C−C distance increases to cope with the twisted configuration (Figure S7). As we discuss shortly, these localized states severely hinder the electron transport.

We next turn to the interaction of the twisted GNRs with BNNTs. The pristine and defective 7-GNRs which twist at 0.50π rad/unit are encapsulated into a (12,12)-BNNT, with optimized geometries depicted in Figure S8a,b. The DOS of the composite system (Figure S8c) indicates that the GNR-BNNT interaction is minimal, and the electronic properties near the Fermi level are not affected at all. A similar study is performed for pristine and defective 12-GNRs twisted at 0.25π rad/unit encapsulated inside a (16,16)-BNNT. The optimized geometries can be seen in Figure S8d,e. As expected, a comparison of the DOS of the hybrid composite and the isolated components also reveals a null interaction, similar to their planar counterpart (Figure S8f).

Electron Transport of Planar and Twisted GNRs. The electron transport characteristics are also investigated for the planar and twisted configuration of all GNRs, with the modeled device configuration depicted in Figure S9. Figure 4a shows the transmission function (TF) of the pristine and defective 7-GNRs both in their planar and twisted configuration. At the charge neutrality point, the TF of the planar, nondefective 7-GNR exhibits a step-like behavior in the available conducting channels. A quantum conductance of $2G_0$ ($G_0 = 2e^2/h$) is observed around the FL with a conductance gap of 0.8 eV. Once the ribbon is twisted, a reduction in the TF is observed at the valence and conduction bands, with the TF being less pronounced at energies near the FL and slowly increasing at around ±1 eV. This has a significant effect on the current−voltage ($I-V$) characteristics as seen in Figure 4b. The planar 7-GNR achieves a current of 8.2 μA at 1.7 V, while the twisted configuration yields only 3.0 μA at similar bias, a 63% reduction in current. The defective 7-GNR exhibits a completely different TF in comparison with the pristine case; here, the conductance gap is ∼0.9 eV, but there is a significant reduction in conductance at the valence band, whereas at the conduction band, the conductance is reduced to $\sim 1G_0$, half the value of the nondefective counterpart. As a result, the defective 7-GNR achieves only 0.9 μA at 1.7 V, 89% lower than the nondefective 7-GNR. After twisting, the TF for a defective 7-GNR is reduced even further at the conduction band, resulting in a current of 0.6 μA at 1.7 V, 93% lower in comparison to the 7-GNR. A summary is presented in Table 1.

Table 1. Band gap (E_g), Current at 1.7 V, and Twist Energy of Pristine and Defective 7- and 12-GNRs

system	E_g (eV)	current at 1.7 V (μA)	twist energy (eV)
7-GNR	0.92	8.2	
defective 7-GNR	1.52	0.9	
twisted 7-GNR	1.41	3.0	2.0
twisted defective 7-GNR	1.18	0.6	2.4
12-GNR	0.43	41.4	
defective 12-GNR	0.75	16.2	
twisted 12-GNR	0.62	23.3	3.5
twisted defective 12-GNR		2.2	5.0

For the 12-GNR case, the pristine and defective 12-GNR exhibits a conductance gap of 0.4 eV (Figure 4c). However, the defective ribbon has a significant reduction in the TF at the valence and conduction bands with results similar to the 7-GNR counterpart. After twisting both nanoribbons, the TF is reduced as expected, and only the twisted and defective 12-GNR exhibits an increase in the conductance gap of 0.77 eV, resulting in a larger turn-on voltage as observed in the $I-V$ curve in Figure 4f. The current achieved at 1.7 V is reduced by 44, 61, and 95% for the twisted, defective, and twisted-defective 12-GNR, respectively, in comparison with the planar, nondefective 12-GNR.

In summary, theoretical modeling for the interaction of encapsulated GNRs with a host BNNT is presented. The results reveal that encapsulated GNRs do not interact with the host BNNT and that the electronic property of the hybrid

DOI: 10.1021/acsomega.8b01617
ACS Omega 2018, 3, 12930−12935

system is simply a mixture of two noninteracting systems. The presence of structural defects (five and seven member rings) and twisting of GNRs significantly compromises the electron transport, but in general, it does not have any effect on the interaction between the encapsulated GNRs and the host BNNT. The origin of twisting is suggested to be the local defective sites at the junction of the GNR fragments. The isolation of a GNR inside the inner cavity of the electrically insulating BNNT provides a route for a possible implementation of GNRs in complex electronic devices, in which the BNNT also acts as a chemically robust protection layer for the encapsulated GNR.

COMPUTATIONAL METHOD

Electronic Properties. The electronic properties are investigated using the DFT within the generalized gradient approximation with the Perdew, Burke, and Ernzerhof parametrization[37] as implemented in the SIESTA code.[38] The valence electrons are represented by a linear combination of pseudo-atomic numerical orbitals using a double-ζ polarized basis.[39] The real-space grid used for charge and potential integration is equivalent to a plane wave cut-off energy of 250 Ry. Periodic boundary conditions are used, and a distance of 25 Å is used to avoid lateral interactions. The Brillouin zones are sampled only at the Γ point during geometric relaxation; however, a K-grid of $1 \times 1 \times 16$ is used to obtain the DOS. All systems are relaxed using a variable cell scheme by conjugate gradient minimization until the maximum force is <0.04 eV/Å. Note that dispersion forces are not considered during the structural optimization, and the addition of such forces is not expected to alter the final configuration.

Electronic Transport. The electronic transport characteristics are investigated by the nonequilibrium Green's function techniques[40] within the Keldysh formalism using the Atomistix ToolKit 2016.4 software.[41] The electronic transport calculations are performed by obtaining well-converged electrodes using the $1 \times 1 \times 301$ Monkhorst–Pack K-grid for sampling the 1D-Brillouin zone and $1 \times 1 \times 101$ K-grid for the scattering region. A real-space grid of 250 Ry and single-ζ polarized (SZP) basis are used. Previous studies have confirmed that the use of such an SZP basis size is appropriate for carbon-based systems.[42,43] The devices consist of a two-probe system where coronene-based nanoribbons (8.65 Å) are used as semi-infinite left and right electrodes. The scattering region consists of pristine and defective GNRs with a total length of ∼34 Å, and for twisted GNRs, the scattering regions have a length of ∼50 Å.

Charge Analysis. The Bader charge analysis[44,45] is used to determine the transferred electronic charge among components using the optimized geometries and 250 Ry as energy cutoff for the real-space grid. The charge density difference $\delta n(r)$ is obtained by subtracting the charge densities of the individual components (GNR and BNNT) from the composite systems, $\delta n(r) = n(r)_{\text{Total}} - n(r)_{\text{GNR}} - n(r)_{\text{BNNT}}$. The charge densities of the isolated components are computed by maintaining the geometry in the composite system.

ASSOCIATED CONTENT

Supporting Information

The Supporting Information is available free of charge on the ACS Publications website at DOI: 10.1021/acsomega.8b01617.

DOS of 7-GNRs, optimized geometry of 12-GNRs, electronic properties of the pure 4-zigzag and 7-armchair GNR, twisted geometry of GNR, and their DOS (PDF)

AUTHOR INFORMATION

Corresponding Authors

*Email: hamid.barzegar@umu.se (H.R.B.).
*Email: azettl@berkeley.edu (A.Z.).

ORCID

Eduardo Gracia-Espino: 0000-0001-9239-0541
Hamid Reza Barzegar: 0000-0002-1314-5407

Notes

The authors declare no competing financial interest.

ACKNOWLEDGMENTS

E.G.-E. and H.R.B. acknowledge support from the Carl Tryggers foundation (CTS-16-161). This work was supported in part by the Swedish Research Council (grant 2015-00520), which provided support for H.R.B. This work was supported in part by the Director, Office of Science, Office of Basic Energy Sciences, Materials Sciences and Engineering Division, of the U.S. Department of Energy under contract no. DE-AC02-05-CH11231, within the sp^2-Bonded Materials Program (KC2207), which provided for postdoctoral assistance in formulation of the problem and writing of the manuscript; and the Department of the U.S. Navy, Office of Naval Research under grant no. N00014-16-1-2229, which provided for correlation of theoretical results to experimental observations. The theoretical simulations were performed on resources provided by the Swedish National Infrastructure for Computing (SNIC) at the High Performance Computing Center North (HPC2N).

REFERENCES

(1) Ezawa, M. Peculiar width dependence of the electronic properties of carbon nanoribbons. *Phys. Rev. B: Condens. Matter Mater. Phys.* **2006**, *73*, 045432.
(2) Wassmann, T.; Seitsonen, A. P.; Saitta, A. M.; Lazzeri, M.; Mauri, F. Clar's Theory, π-Electron Distribution, and Geometry of Graphene Nanoribbons. *J. Am. Chem. Soc.* **2010**, *132*, 3440–3451.
(3) Yang, L.; Park, C.-H.; Son, Y.-W.; Cohen, M. L.; Louie, S. G. Quasiparticle energies and band gaps in graphene nanoribbons. *Phys. Rev. Lett.* **2007**, *99*, 186801.
(4) Nakada, K.; Fujita, M.; Dresselhaus, G.; Dresselhaus, M. S. Edge state in graphene ribbons: Nanometer size effect and edge shape dependence. *Phys. Rev. B: Condens. Matter Mater. Phys.* **1996**, *54*, 17954–17961.
(5) Son, Y.-W.; Cohen, M. L.; Louie, S. G. Energy gaps in graphene nanoribbons. *Phys. Rev. Lett.* **2006**, *97*, 216803.
(6) Prezzi, D.; Varsano, D.; Ruini, A.; Molinari, E. Quantum dot states and optical excitations of edge-modulated graphene nanoribbons. *Phys. Rev. B: Condens. Matter Mater. Phys.* **2011**, *84*, 041401.
(7) Sevincli, H.; Topsakal, M.; Ciraci, S. Superlattice structures of graphene-based armchair nanoribbons. *Phys. Rev. B: Condens. Matter Mater. Phys.* **2008**, *78*, 245402.
(8) Xu, Z.; Zheng, Q.-S.; Chen, G. Elementary building blocks of graphene-nanoribbon-based electronic devices. *Appl. Phys. Lett.* **2007**, *90*, 223115.
(9) Han, M. Y.; Ozyilmaz, B.; Zhang, Y. B.; Kim, P. Energy band-gap engineering of graphene nanoribbons. *Phys. Rev. Lett.* **2007**, *98*, 206805.
(10) Chen, Z.; Lin, Y.-M.; Rooks, M. J.; Avouris, P. Graphene nanoribbon electronics. *Physica E* **2007**, *40*, 228–232.

DOI: 10.1021/acsomega.8b01617
ACS Omega 2018, 3, 12930–12935

(11) Kosynkin, D. V.; Higginbotham, A. L.; Sinitskii, A.; Lomeda, J. R.; Dimiev, A.; Price, B. K.; Tour, J. M. Longitudinal unzipping of carbon nanotubes to form graphene nanoribbons. *Nature* **2009**, *458*, 872−876.
(12) Jiao, L.; Zhang, L.; Wang, X.; Diankov, G.; Dai, H. Narrow graphene nanoribbons from carbon nanotubes. *Nature* **2009**, *458*, 877−880.
(13) Jiao, L.; Wang, X.; Diankov, G.; Wang, H.; Dai, H. Erratum: Facile synthesis of high-quality graphene nanoribbons. *Nat. Nanotechnol.* **2011**, *6*, 132.
(14) Talyzin, A. V.; Anoshkin, I. V.; Krasheninnikov, A. V.; Nieminen, R. M.; Nasibulin, A. G.; Jiang, H.; Kauppinen, E. I. Synthesis of graphene nanoribbons encapsulated in single-walled carbon nanotubes. *Nano Lett.* **2011**, *11*, 4352−4356.
(15) Chamberlain, T. W.; Biskupek, J.; Rance, G. A.; Chuvilin, A.; Alexander, T. J.; Bichoutskaia, E.; Kaiser, U.; Khlobystov, A. N. Size, structure, and helical twist of graphene nanoribbons controlled by confinement in carbon nanotubes. *Acs Nano* **2012**, *6*, 3943−3953.
(16) Chuvilin, A.; Bichoutskaia, E.; Gimenez-Lopez, M. C.; Chamberlain, T. W.; Rance, G. A.; Kuganathan, N.; Biskupek, J.; Kaiser, U.; Khlobystov, A. N. Self-assembly of a sulphur-terminated graphene nanoribbon within a single-walled carbon nanotube. *Nat. Mater.* **2011**, *10*, 687−692.
(17) Cai, J.; Ruffieux, P.; Jaafar, R.; Bieri, M.; Braun, T.; Blankenburg, S.; Muoth, M.; Seitsonen, A. P.; Saleh, M.; Feng, X.; Müllen, K.; Fasel, R. Atomically precise bottom-up fabrication of graphene nanoribbons. *Nature* **2010**, *466*, 470−473.
(18) Wang, X.-Y.; Urgel, J. I.; Barin, G. B.; Eimre, K.; Di Giovannantonio, M.; Milani, A.; Tommasini, M.; Pignedoli, C. A.; Ruffieux, P.; Feng, X.; Fasel, R.; Müllen, K.; Narita, A. Bottom-up synthesis of heteroatom-doped chiral graphene nanoribbons. *J. Am. Chem. Soc.* **2018**, *140*, 9104−9107.
(19) Chen, Y.-C.; de Oteyza, D. G.; Pedramrazi, Z.; Chen, C.; Fischer, F. R.; Crommie, M. F. Tuning the band gap of graphene nanoribbons synthesized from molecular precursors. *Acs Nano* **2013**, *7*, 6123−6128.
(20) Chen, Y.-C.; Cao, T.; Chen, C.; Pedramrazi, Z.; Haberer, D.; de Oteyza, D. G.; Fischer, F. R.; Louie, S. G.; Crommie, M. F. Molecular bandgap engineering of bottom-up synthesized graphene nanoribbon heterojunctions. *Nat. Nanotechnol.* **2015**, *10*, 156−160.
(21) Chernov, A. I.; Fedotov, P. V.; Anoshkin, I. V.; Nasibulin, A. G.; Kauppinen, E. I.; Kuznetsov, V. L.; Obraztsova, E. D. Single-walled carbon nanotubes as a template for coronene stack formation. *Phys. Status Solidi B* **2014**, *251*, 2372−2377.
(22) Verberck, B.; Okazaki, T.; Tarakina, N. V. Ordered and disordered packing of coronene molecules in carbon nanotubes. *Phys. Chem. Chem. Phys.* **2013**, *15*, 18108−18114.
(23) Mandal, B.; Sarkar, S.; Sarkar, P. Energetics and electronic structure of encapsulated graphene nanoribbons in carbon nanotube. *J. Phys. Chem. A* **2013**, *117*, 8568−8575.
(24) Ilyasov, V. V.; Meshi, B. C.; Nguyen, V. C.; Ershov, I. V.; Nguyen, D. C. Edge and substrate-induced bandgap in zigzag graphene nanoribbons on the hexagonal nitride boron 8-ZGNR/h-BN(0001). *AIP Adv.* **2013**, *3*, 092105.
(25) Zhang, W.; Hajiheidari, F.; Li, Y.; Mazzarello, R. Electronic and magnetic properties of H-terminated graphene nanoribbons deposited on the topological insulator Sb2Te3. *Sci. Rep.* **2016**, *6*, 29009.
(26) Barzegar, H. R.; Pham, T.; Talyzin, A. V.; Zettl, A. Synthesis of graphene nanoribbons inside boron nitride nanotubes. *Phys. Status Solidi B* **2016**, *253*, 2377−2379.
(27) Rubio, A.; Corkill, J. L.; Cohen, M. L. Theory of graphitic boron nitride nanotubes. *Phys. Rev. B: Condens. Matter Mater. Phys.* **1994**, *49*, 5081−5084.
(28) Lai, L.; Song, W.; Lu, J.; Gao, Z.; Nagase, S.; Ni, M.; Mei, W. N.; Liu, J.; Yu, D.; Ye, H. Structural and electronic properties of fluorinated boron nitride nanotubes. *J. Phys. Chem. B* **2006**, *110*, 14092−14097.
(29) Gracia-Espino, E.; Jia, X.; WÅgberg, T. Improved oxygen reduction performance of Pt-Ni nanoparticles by adhesion on nitrogen-doped graphene. *J. Phys. Chem. C* **2014**, *118*, 2804−2811.
(30) Lim, D.-H.; Wilcox, J. Mechanisms of the oxygen reduction reaction on defective graphene-supported Pt nanoparticles from first-principles. *J. Phys. Chem. C* **2012**, *116*, 3653−3660.
(31) Yu, M.-F.; Dyer, M.; Chen, J.; Qian, D.; Liu, W.; Ruoff, R. S. Locked twist in multiwalled carbon-nanotube ribbons. *Phys. Rev. B: Condens. Matter Mater. Phys.* **2001**, *64*, 241403.
(32) Li, X.; Wang, X.; Zhang, L.; Lee, S.; Dai, H. Chemically derived, ultrasmooth graphene nanoribbon semiconductors. *Science* **2008**, *319*, 1229−1232.
(33) Shenoy, V. B.; Reddy, C. D.; Ramasubramaniam, A.; Zhang, Y. W. Edge-stress-induced warping of graphene sheets and nanoribbons. *Phys. Rev. Lett.* **2008**, *101*, 245501.
(34) Bets, K. V.; Yakobson, B. I. Spontaneous twist and intrinsic instabilities of pristine graphene nanoribbons. *Nano Res.* **2009**, *2*, 161−166.
(35) Barzegar, H. R.; Yan, A.; Coh, S.; Gracia-Espino, E.; Ojeda-Aristizabal, C.; Dunn, G.; Cohen, M. L.; Louie, S. G.; WÅgberg, T.; Zettl, A. Spontaneous twisting of a collapsed carbon nanotube. *Nano Res.* **2017**, *10*, 1942−1949.
(36) Banhart, F. Graphene nanoribbons: Twisted within nanotubes. *Nat. Mater.* **2011**, *10*, 651−652.
(37) Perdew, J. P.; Ruzsinszky, A.; Csonka, G. I.; Vydrov, O. A.; Scuseria, G. E.; Constantin, L. A.; Zhou, X. L.; Burke, K. Restoring the density-gradient expansion for exchange in solids and surfaces. *Phys. Rev. Lett.* **2009**, *102*, 136406.
(38) Soler, J. M.; Artacho, E.; Gale, J. D.; García, A.; Junquera, J.; Ordejón, P.; Sánchez-Portal, D. The SIESTA method forab initioorder-Nmaterials simulation. *J. Phys.: Condens. Matter* **2002**, *14*, 2745−2779.
(39) Junquera, J.; Paz, O.; Sanchez-Portal, D.; Artacho, E. Numerical atomic orbitals for linear-scaling calculations. *Phys. Rev. B: Condens. Matter Mater. Phys.* **2001**, *64*, 235111.
(40) Taylor, J.; Guo, H.; Wang, J. Ab initio modeling of quantum transport properties of molecular electronic devices. *Phys. Rev. B: Condens. Matter Mater. Phys.* **2001**, *63*, 245407.
(41) Brandbyge, M.; Mozos, J.-L.; Ordejon, P.; Taylor, J.; Stokbro, K. Density-functional method for nonequilibrium electron transport. *Phys. Rev. B: Condens. Matter Mater. Phys.* **2002**, *65*, 165401.
(42) Topsakal, M.; Bagci, V. M. K.; Ciraci, S. Current-voltage (I-V) characteristics of armchair graphene nanoribbons under uniaxial strain. *Phys. Rev. B: Condens. Matter Mater. Phys.* **2010**, *81*, 205437.
(43) Gracia-Espino, E.; López-Urías, F.; Terrones, H.; Terrones, M. Electron transport study on functionalized armchair graphene nanoribbons: DFT calculations. *RSC Adv.* **2016**, *6*, 21954−21960.
(44) Tang, W.; Sanville, E.; Henkelman, G. A grid-based Bader analysis algorithm without lattice bias. *J. Phys.: Condens. Matter* **2009**, *21*, 084204.
(45) Sanville, E.; Kenny, S. D.; Smith, R.; Henkelman, G. Improved grid-based algorithm for Bader charge allocation. *J. Comput. Chem.* **2007**, *28*, 899−908.

DOI: 10.1021/acsomega.8b01617
ACS Omega 2018, 3, 12930−12935